ELSEVIER

Earth and Planetary Science Letters 204 (2002) 101–113

EPSL

www.elsevier.com/locate/epsl

Depressurization of fine powders in a shock tube and dynamics of fragmented magma in volcanic conduits

B. Cagnoli [a,*], A. Barmin [b], O. Melnik [a,b], R.S.J. Sparks [a]

[a] *Centre for Environmental and Geophysical Flows, Department of Earth Sciences, University of Bristol, Bristol BS8 1RJ, UK*
[b] *Institute of Mechanics, Moscow State University, 1-112b Mitchurinski prosp., Moscow, Russia*

Received 19 April 2002; received in revised form 7 August 2002; accepted 4 September 2002

Abstract

Samples of fine glass beads (mean grain size equal to 38 and 95 μm) have been depressurized within a vertical shock tube. These short-lived, rapid decompressions resemble discrete, cannon-like vulcanian explosions and produce two-phase flows that are inhomogeneous in density in both vertical and horizontal directions because of the presence of bubble-like heterogeneities. We suggest that also volcanic flows may present similar inhomogeneities in density. In the experimental apparatus the flow velocities increase from approximately 1 to 13 m/s when the pressure drop increases from approximately 200 to 900 mbar. A physical model of the initial velocities of expansions in the shock tube has been applied to a range of volcanic overpressures between 0.1 and 20 MPa, suggesting initial velocities of volcanic flows caused by the removal of a rock plug in volcanic conduits between 25 and 400 m/s. During the experiments at large pressure drops, as the mixture expands and moves up the tube, the flow front becomes highly irregular and bubble-like heterogeneities form. The shape of these bubbles becomes distorted and stretched in the turbulent flow. During the experiments at relatively small pressure drops, the sample oscillates when the particles, after the expansion, flow back and bounce upward again. Jets with diameter smaller than that of the tube are ejected from the oscillating samples generating independent pulses. Large bubble-like heterogeneities whose diameter is a significant fraction of the tube diameter can also discretize the flows. Similar mechanisms in real volcanoes may produce pulse-like ejections of gas–particle mixtures out of the vent.

Keywords: volcanism; shock tube experiments; pyroclastic flows

1. Introduction

We present the results of shock tube experiments involving depressurization of fine powders. The behavior of these powders could shed light on the dynamics of gas–particle flows in volcanic conduits. The explosive expansion of mixtures of pressurized gases and fragments of magma within volcanic conduits and volcanic flows cannot be studied directly. Several studies suggest possible dynamics using laboratory simulations [1–9]. The advantages of experimental studies with analogue systems are that high velocity gas–particle

* Corresponding author. Present address: Earth and Planetary Science, University of California, Berkeley, 307 McCone Hall, Berkeley, CA 94720-4767, USA. Tel.: +1-510-642-2288; Fax: +1-510-643-9980.
E-mail address: cagnoli@seismo.berkeley.edu (B. Cagnoli).

0012-821X/02/$ – see front matter
PII: S0012-821X(02)00952-4

flows can be observed directly and complex phenomena (not yet identified by computer simulations or observations of volcanic eruptions) can be recognized. Laboratory experiments can also be used to validate theoretical results.

Our experiments develop and expand the studies made by Anilkumar and co-authors [1,2]. Here, we used finer grain size particles (average particle diameters are 38 μm and 95 μm) than those used by them in corresponding experiments (125, 180, 250 and 500 μm). We also made decompressions through a wider range of pressure drops (from approximately 900 to 200 mbar) instead of the single larger pressure drop values (1 and 2.1 bar) used by Anilkumar et al. [1,2]. Furthermore, in almost all their experiments the samples rested on a mesh screen. In only two of their experiments [2] the beds rested on the closed bottom end of the sample holder as in all our decompressions.

The present study is motivated by situations in volcanoes where pressurized gases expand through an initially concentrated dispersion of particles. One important case is in volcanic conduits where magma fragmentation occurs over a narrow depth region and a mixture of pyroclasts and gas expands and accelerates up the conduit. Another comparable situation is when a lava dome containing pressurized gases collapses, initiating magma fragmentation within the conduit. In this case the gas phase expands as the rock mass of the dome disintegrates. Pyroclastic flows can be generated in both situations and for this reason our experiments can be useful in understanding their formation. This research aims at studying the behavior of gas–particle flows in volcanic conduits immediately after magma fragmentation in explosive eruptions. Our quantitative analysis focuses on the early stages of the expansions and the paper ends with a discussion of the applications and implications of the experimental observations for volcanic eruptions.

2. Method

Beds of fine grain size glass beads (with density $\sim$2500 kg/m^3) were suddenly depressurized in a vertical shock tube and their behavior recorded using a high-speed video camera at 2000 frames per second. We have used fine powders because the diameter of the flow channel in an experimental apparatus should be large enough to allow for the large range of scales in the flow behaviors as in natural flows [1–4]. In other words, as in volcanic conduits, the ratio between the diameter of the particle and the diameter of the tube has been kept as small as possible. The shock tube apparatus consists of a cylindrical low-pressure tank (50 cm in diameter and 1 m high) and a vertical Pyrex™ test cell at the bottom end of which the sample rests at atmospheric pressure (Fig. 1). A plastic diaphragm is positioned between the tank and the test cell and is electrically removed by sudden melting to initiate the decompressions. The low pressure within the low-pressure tank is generated with a pump and measured using a pressure transducer.

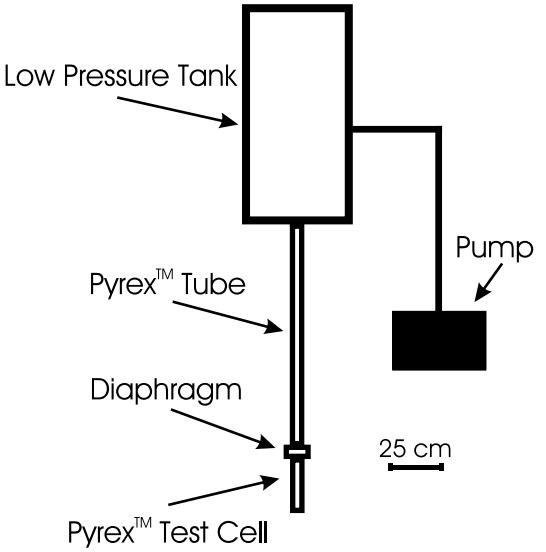

Fig. 1. Sketch of the experimental apparatus. The sample in the Pyrex™ test cell is at atmospheric pressure. The interior of the tank and Pyrex™ tube is at pressure lower than atmospheric.

These decompressions have been carried out at different pressure drops (Δp), defined as the pressure difference across the diaphragm between test cell and low-pressure tank. Sets of experiments have been carried out at 100 mbar incremental steps from Δp approximately equal to 200 mbar

to Δp approximately equal to 900 mbar. These pressure drop values have then been corrected taking into account the daily variations of atmospheric pressure. For this reason, some experiments were made at slightly different pressure drops than the others. Each single experiment in the same experimental conditions and at the same pressure drop has been repeated two or three times in order to assess its reproducibility (Table 1). The environment has been kept as dry as possible during the experiments (average relative humidity of the air equal to 25% and average room temperature equal to 27°C) in order to prevent cohesive behavior of the powders.

The main sets of experiments were carried out using fine grain size particles with a mean diameter of 38 μm (standard deviation 14 μm) in a test cell that is 23 cm long and approximately 3.8 cm in internal diameter. In two ancillary sets of experiments we (1) respectively depressurized the same grain size particles in a narrower test cell (47 cm long and 1.6 cm in internal diameter) and (2) depressurized in the same test cell coarser grain size particles (mean diameter 95 μm; standard deviation 30 μm). These ancillary experiments are intended for the detection of major qualitative differences in the flow behavior when the mean diameter of the particles is approximately doubled or the diameter of the test cell is approximately halved. In the large diameter test cell we used different amounts of powder, 100, 150 and 200 g, which result in samples that are respectively about 6.5, 9.5 and 12.5 cm in height. The samples in the narrower test cell are 36 cm in height (100 g of powder). Table 1 summarizes the characteristics of samples and experiments.

3. Results

3.1. Experiments with the large diameter test cell and fine grain size (38 μm) powders

The sets of experiments L, M and N were conducted in the large diameter test cell with the fine grain size (38 μm) powders. Fig. 2 presents a sequence of images showing the typical large Δp expansion (approximately between 900 and 500 mbar) of a sample with the generation of bubble-like heterogeneities in a flow that becomes gradually more turbulent and inhomogeneous. The expansion appears initially quite uniform with a nearly horizontal upper surface and no discernible bubbles. As the mixture expands and moves further up the tube the flow front becomes more irregular and the bubble-like heterogeneities form in the expanding bed. These bubbles tend to become bigger (up to 1 cm in diameter at Δp approximately equal to 900 mbar), more distorted and stretched as the bed expands into a turbulent flow. Fig. 2 also shows that the expanding bed is vertically zoned with no visible bubbles at the

Table 1
Characteristics of samples and experiments

Name of the set of experiments	Mean grain size	Powder bed		Test cell		Froude number range[a]	Runs at each Δp[b]
	(μm)	height (cm)	weight (g)	height (cm)	∅[c] (cm)		
L	38	9.5	150	23	3.8	93–3	3
M	38	12.5	200	23	3.8	80–3	3
N	38	6.5	100	23	3.8	111–3	3
P	38	36	100	47	1.6	41–0.4	2
Q	95	9.5	150	23	3.8	74–1	2

[a] The Froude number is computed taking into account the height of the samples after 6 ms from the beginning of the expansions. The large value of the range corresponds to the experiments at the largest Δp and the small one to the experiments at the smallest Δp in each set. Intermediate Δp experiments present intermediate Froude numbers.
[b] Number of experiments repeated at the same Δp in each set of experiments.
[c] Internal diameter.

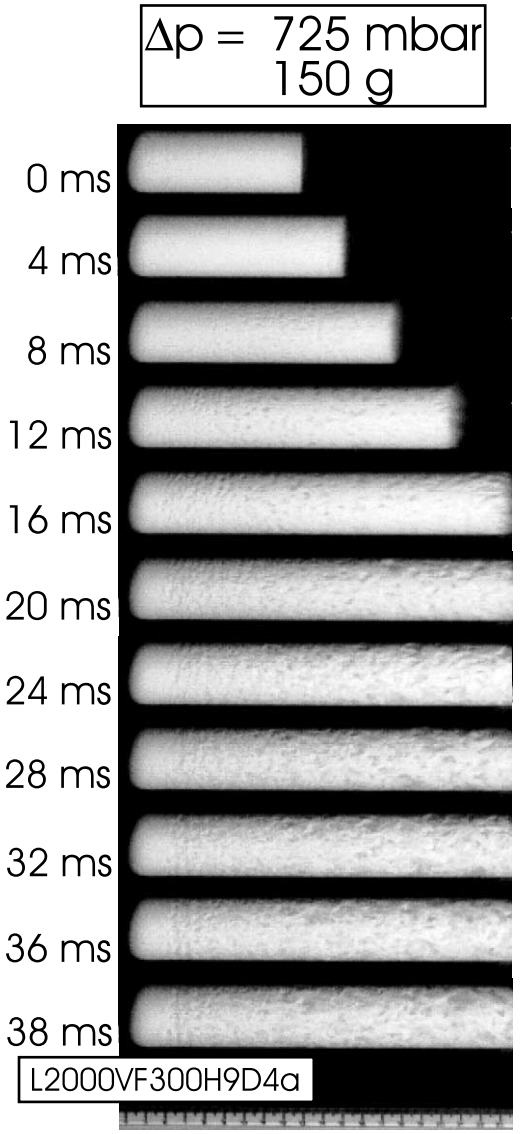

Fig. 2. These frames show a decompression that has been carried out at relatively large pressure drop (Δp). The value in g is the weight of the sample. The time in ms is measured from the beginning of the expansion. The mean grain size is 38 μm. The marks along the length scale are cm and half cm. The test cell was vertical during the experiments.

base. These bubble-like heterogeneities can be seen only a few centimeters above the bottom of the test cell and become larger, more distorted and expanded with increasing distance from the base. Sub-horizontal concentrations of gas-rich regions are also observable between the basal zone with no discernible bubbles and the upper zone with bubbles (Fig. 2). Fig. 3 shows other examples of flows which are inhomogeneous in both vertical and horizontal directions, and whose flow fronts are highly irregular with finger-like protrusions. At the end of the large Δp expansions, the highly dispersed particles flow back and settle at the bottom of the test cell.

At relatively small Δp (between approximately 400 and 200 mbar) the particle–gas mixture moves

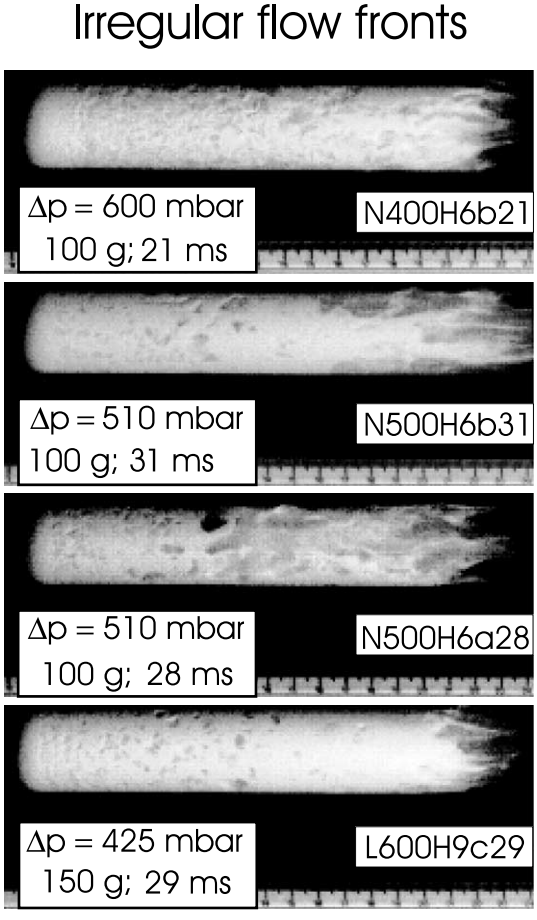

Fig. 3. Four images of different experiments showing highly irregular flow fronts with finger-like protrusions. The pressure difference between tank and test cell is Δp. The value in g is the weight of the sample. The time in ms is measured from the beginning of the expansion. The marks along the length scale are cm and half cm. The mean grain size is 38 μm. The test cells were vertical during the experiments.

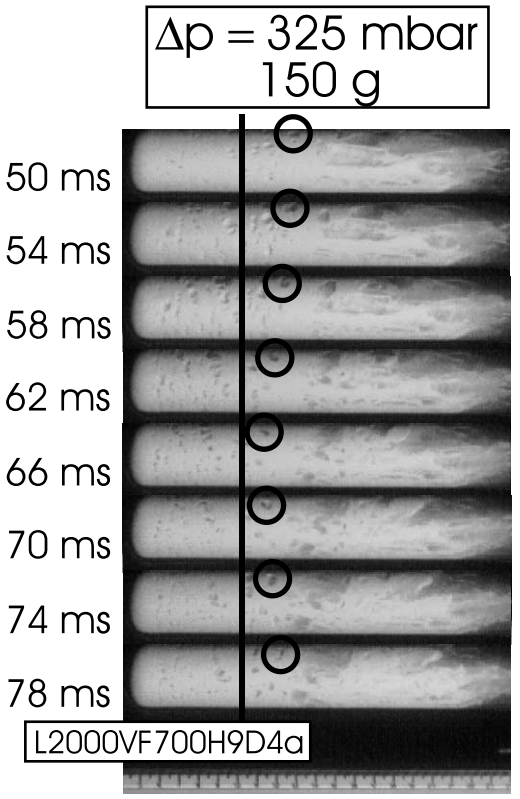

Fig. 4. Sequence of frames whose time after beginning of expansion is shown in ms. It shows that the sample is oscillating (the circle highlights an oscillating bubble). The pressure drop is Δp. The value in g is the weight of the sample. The mean grain size is 38 μm. The marks along the length scale are cm and half cm. The test cell was vertical during the experiments.

up the tube and then flows back toward the bottom end of the test cell and bounces upward again. This happens more than once and results in oscillations of the samples (Fig. 4), whose amplitude decreases in time. The oscillations project upward jets that detach themselves from the main body of the sample. For example, Fig. 5 shows two jets that behave independently within the same tube (one is moving upward and the other one is flowing back). The jets generated by the oscillations are independent pulses with a diameter smaller than that of the tube (Fig. 5). The flow fronts are highly irregular also at relatively small Δp. The characteristics described above for large and small Δp apply similarly to the experiments with 100, 150 and 200 g samples.

3.2. *Experiments with the large diameter test cell and coarse grain size (95 μm) powders*

The set of experiments Q involved the large diameter test cell and coarser grain size (95 μm) powders. Again, at large Δp, the particle bed expands turbulently with the formation of bubble-like heterogeneities and the particles fall back without oscillations. However, at small Δp between approximately 400 and 200 mbar the oscillations are observed, but the jets are less spectacular and much smaller in size than those obtained with finer grain size particles. Again, sub-horizon-

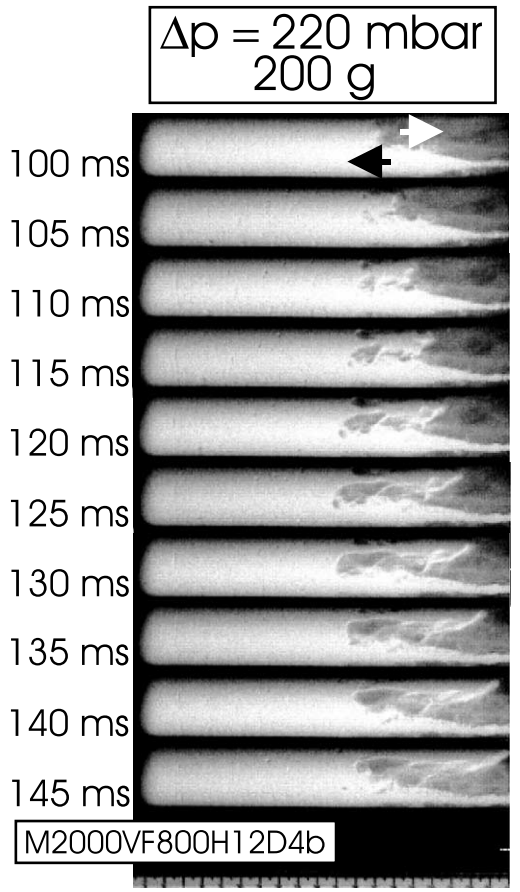

Fig. 5. This sequence of frames shows a jet moving upward (white arrow) and a jet flowing back (black arrow). The pressure drop is Δp. The time in ms is measured from the beginning of the expansion. The value in g is the weight of the sample. The marks along the length scale are cm and half cm. The mean grain size is 38 μm. The test cell was vertical during the experiments.

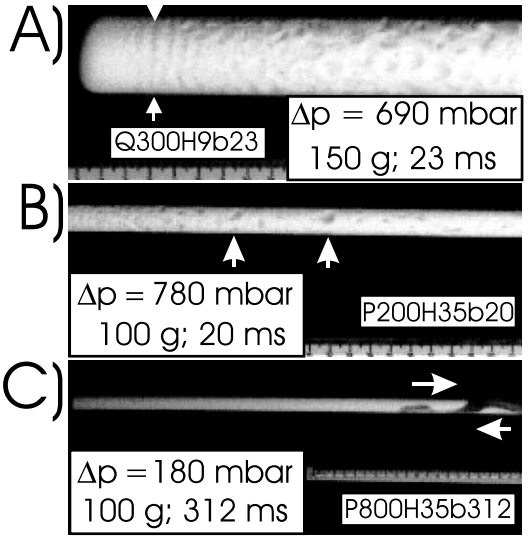

Fig. 6. Frame A shows sub-horizontal concentrations of voids (between the white arrows) formed during the decompression at relatively large pressure drops of a sample with coarser grain size particles (95 μm). Frames B and C are images from experiments carried out using the narrow tube and finer grain size particles (38 μm). A flow discretized by relatively large bubble-like heterogeneities is visible in frame B and a flow discretized by jets in frame C. In particular, frame C shows one jet moving upward and one jet flowing back (arrows). The pressure drop is Δp. The time in ms is the time from the beginning of the expansion. The value in g is the weight of the sample. The marks along the length scale are cm and half cm. The test cells were vertical during the decompressions.

tal concentrations of gas-rich regions split a portion of the bed horizontally (Fig. 6A). Here, this feature, which is located between the upper part of the bed with bubbles and the lower one without visible bubbles, is more prominent than in the finer grain size samples.

3.3. Experiments with the narrow test cell and fine grain size (38 μm) powders

The set of experiments P were carried out with the narrow test cell and fine grain size (38 μm) powders. Again, the oscillations of the samples are best developed at small Δp (200 and 300 mbar). At large Δp (900 and 800 mbar) the flows are broken by relatively large bubble-like heterogeneities whose diameter is a substantial fraction of that of the tube (Fig. 6B). The oscillations of the sample generate jets, which behave independently when produced in sequence (Fig. 6C).

3.4. Initial velocities and initial accelerations

The positions versus time of the most advanced point of the flow fronts have been measured using high-speed videography. These measurements allow estimates of an initial average velocity of expansion observed within the field of view of the video camera. A couple of examples are presented in Fig. 7. Unfortunately, the limited field of view of the video camera does not include the entire distance traveled by the flows within the shock tube. For this reason our measurements focus on the early stages of the expansions, which consist of an initial acceleration and then a period over which the distance versus time data present a linear trend as visible in Fig. 7 (of course, at later stages, these powders decelerate and eventually flow back).

The average velocities have been estimated as the slope of a straight line fitting the data by least-square regression in the region of linear distance versus time. The first five points were not used because they show the largest acceleration (Fig. 7). The regression lines were always fitted to the data within the same time window (2.5–6 ms) for all the experiments. This initial time interval is suitable to compare the velocities at different Δp

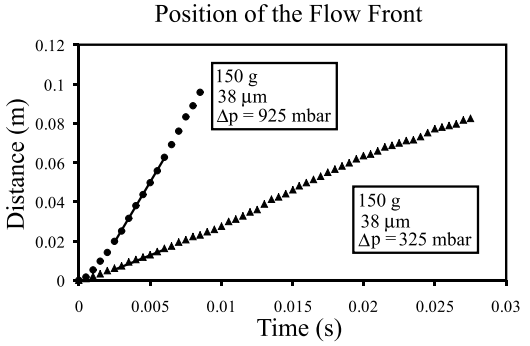

Fig. 7. Positions of flow front versus time during the decompressions of one sample at large Δp (experiment L100a) and one at small Δp (experiment L700a). The value in g is the weight of the sample and the value in μm is the mean grain size. The portion of data in the time window 2.5–6 ms has been fitted with a straight line in a least-square sense to estimate an initial average velocity.

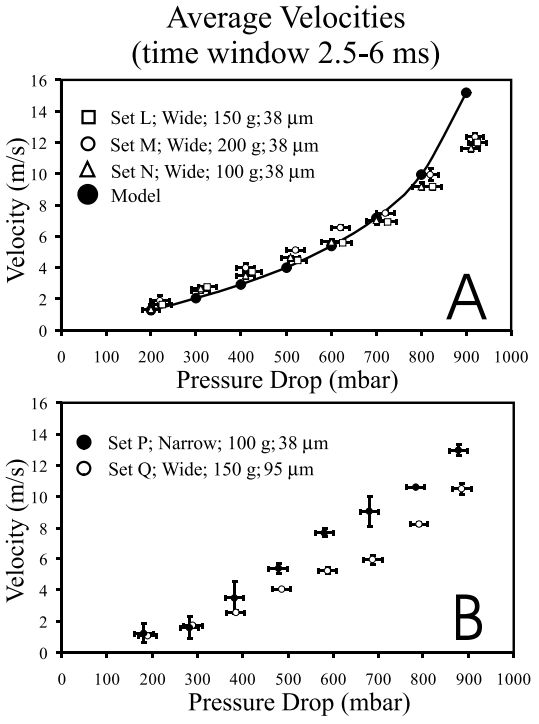

Fig. 8. Average initial velocities of expansion versus pressure drop in the different sets of experiments. The velocities shown here are the mean of the average initial velocities obtained in experiments repeated in the same conditions and at the same pressure drop. The values in g represent the amount of powder. Wide and narrow refer to the diameter of the test cell. The values in µm are the mean grain sizes of the glass beads. The curve shows the theoretical predictions obtained from our model of the initial velocities of expansion of the gas–particle flows of the fine grain size particles in the large diameter test cell.

because the flow fronts are less irregular and the samples at small Δp are not oscillating yet. The evaluation of the flow front position becomes more uncertain as the front becomes more irregular and distorted.

Fig. 8 presents the initial velocities of expansion versus the different pressure drops in the different sets of experiments. The values plotted in these figures are the mean of the average velocities of the experiments that were repeated exactly in the same conditions and at the same pressure drops (the vertical error bar represents the standard error of the mean). The horizontal error bar represents an estimate of the experimental and measurement uncertainties in the determination of the pressure drop. These uncertainties could be due to possible leakage of the low-pressure tank or possible calibration errors of the pressure meter. Fig. 8 shows that in all sets of experiments the velocity increases as the pressure drop increases (the range is approximately between 1 and 13 m/s). Our movies also allow estimates of the initial average accelerations of the flow fronts during the first 2.5 ms of the expansions, which range from 500 to 50 times the acceleration of gravity (g) at Δp respectively from approximately 900 to 200 mbar (Fig. 9).

4. Model of the initial velocities of expansion in the shock tube

The Froude number is the dimensionless ratio of momentum to gravitational force and is equal to:

$$Fr = \frac{U^2}{gL} \tag{1}$$

where U is the velocity, g the acceleration due to gravity and L is a characteristic length such as the height of the sample bed in the vertical test cell. The acceleration of gravity becomes important when $Fr < 1$. Using the experimental velocities

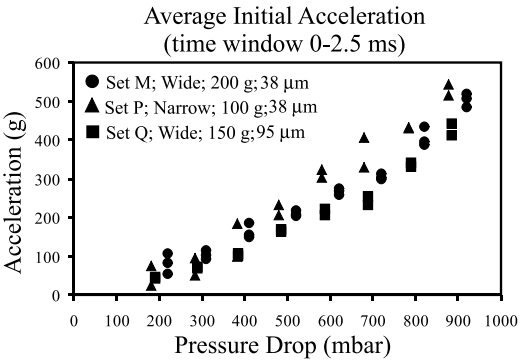

Fig. 9. Average initial accelerations during the first 2.5 ms versus pressure drop in the set of experiments M, P and Q. The same experiment in the same condition and at the same pressure drop was carried out two or three times. The values in g represent the amount of powder. Wide and narrow refer to the diameter of the test cell. The values in µm are the mean grain sizes of the glass beads.

shown above, we have calculated the Froude number for our experiments with L equal to the height of the samples after 6 ms from the beginning of the expansions, because our average velocities are measured in the time window between 2.5 and 6 ms. In this case, the Froude number goes from 111 at large Δp to 1 at small Δp in the short test cell, whereas in the long test cell the Froude number goes from 41 at large Δp down to 0.4 at small Δp (Table 1). Thus, in the early stages of the expansions, most of the experiments are dominated by momentum.

The mathematical model presented here has been developed to describe the physics of the early stages of the expansions in the shock tube. In our model we neglect the effect of gravity because the Froude number (Table 1) shows that its influence is important only for the small Δp decompressions in the long test cell. We also neglect the difference in velocity between particles and gas. The validity of this assumption for the 38 μm glass beads can be verified using the momentum equation for an individual particle written in the following form:

$$\rho_p \frac{\partial U_p}{\partial t} = \frac{1.75(1-\alpha)\rho_g}{\alpha^3 x}(U_g - U_p)^2 + \frac{150\mu_g(1-\alpha)^2}{\alpha^3 x^2}(U_g - U_p) \quad (2)$$

Here the right side of this relationship comes from the Ergun equation [10] for flow through randomly packed beds of monosized spherical particles, where x is their diameter, μ_g is the gas viscosity, α is the bed voidage, ρ_p is the density of the particles and t is time. Assuming that the gas velocity U_g is constant, the initial particle velocity U_p is zero and that there are no changes in the gas density ρ_g and volume concentration of particles $(1-\alpha)$, the time for velocity equilibration (i.e. when $U_p = 0.95 U_g$) is approximately 1–1.5 ms for the 38 μm glass beads, but up to 10 ms for the 95 μm particles. Thus for the purpose of this modeling, we can neglect the difference in velocity between particles and gas after the very first moment of the expansion of the fine grain size glass beads.

After the disruption of the diaphragm in our experimental apparatus, a rarefaction wave propagates into the test cell and a compression shock wave moves upward in the opposite direction. Between these waves there is an expanding region of constant pressure P_{SR} and velocity U_{SR} [11]. Their values can be computed before the rarefaction wave enters the particle bed by solving the following system of equations [11]:

$$\frac{2}{\gamma-1}\frac{C_0}{C_1}\left[1-\left(\frac{P_{SR}}{P_0}\right)^{\frac{\gamma-1}{2\gamma}}\right] = \left(\frac{P_{SR}}{P_1}-1\right)\sqrt{\frac{1-(\gamma-1)/(\gamma+1)}{\gamma((\gamma-1)/(\gamma+1)+P_{SR}/P_1)}} \quad (3a)$$

$$U_{SR} = \frac{2C_0}{\gamma-1}\left[1-\left(\frac{P_{SR}}{P_0}\right)^{\frac{\gamma-1}{2\gamma}}\right] \quad (3b)$$

Here γ is equal to 1.4 and represents the isentropic exponent of air, P_0 and P_1 are respectively the pressures in the high and low pressure portions of the experimental apparatus and C_0 and C_1 are the velocities of sound calculated for the same portions of the apparatus ($C_i = (\gamma P_i/\rho_i)^{1/2}$, where ρ_i are the densities and $i = 1, 2$).

When the rarefaction wave reaches the top of the sample some of its energy is reflected upward and some propagates into the sample. In correspondence to the latter, the pressure starts decreasing and the air between the particles moves upward at high velocity. To describe the propagation of the rarefaction wave within the expanding bed we need to write the equation of state for the gas–particle mixtures assuming (1) velocity equilibrium between gas and particles and (2) isothermal expansion for the mixture because of the high heat capacity of the tiny particles and the rapid heat transfer between phases. This equation of state and the velocity of sound C_m in the mixture can be written in the following form:

$$P = \frac{\alpha_0 P_0}{(1-\alpha_0)} \frac{\rho_m}{(\rho_p - \rho_m)};\ C_m^2 =$$

$$\frac{\partial P}{\partial \rho_m} = \frac{P_0}{\rho_p} \frac{\alpha_0}{1-\alpha_0} \frac{\rho_p^2}{(\rho_p - \rho_m)^2} \quad (4)$$

where P is the pressure in the mixture, α_0 is the initial volume concentration of gas and ρ_m is the density of the mixture.

It is then possible to compute the velocity U of the flow front in the shock tube by solving the following system of equations [11]:

$$-\sqrt{\frac{P_0 \alpha_0}{\rho_p (1-\alpha_0)}} \ln\left(\frac{P}{P_0}\right) =$$

$$U_{SR} + \frac{2C_0}{\gamma - 1}\left[\left(\frac{P}{P_0}\right)^{\frac{\gamma - 1}{2\gamma}} - \left(\frac{P_{SR}}{P_0}\right)^{\frac{\gamma - 1}{2\gamma}}\right] \quad (5a)$$

$$U = -\sqrt{\frac{P_0 \alpha_0}{\rho_p (1-\alpha_0)}} \ln\left(\frac{P}{P_0}\right) \quad (5b)$$

where Eqs. 5a and 5b have been obtained by applying to the gas–particle mixtures described by Eq. 4 the technique used for Riemann rarefaction waves in perfect gases [11]. The assumption is made that the thickness of the initial rarefaction wave in air is small so that the pressure at the top of the sample is immediately equal to P_{SR} after its passage.

The pressure P in Eqs. 5a and 5b is smaller than the value P_1 in the low-pressure tank as a result of the interaction of the rarefaction wave with the air between diaphragm and sample. For this reason the actual pressure drop applied to the sample ($P_0 - P$) is larger than $P_0 - P_1$. In any case, the velocity U is plotted versus the pressure drop $P_0 - P_1$ in Fig. 8A to allow a comparison with the experimental data. This figure shows that our theoretical predictions are in good agreement with the experimental data. At large pressure drop (Fig. 8A), the predicted values are higher than the experimental ones probably because with high accelerations the difference in velocity between gas and particles becomes more important. Furthermore, the velocities in the narrow test cell (Fig. 8B) are slightly higher than those predicted by the model (Fig. 8A). This is due to the fact that our model refers to the main set of experiments with the large diameter test cell where the diameter of the tube is the same (3.8 cm) above and below the diaphragm. In the experiments carried out with the narrow test cell, the diameter of the test cell below the diaphragm is smaller (1.6 cm) than that of the tube above the diaphragm (3.8 cm). This leads to more gas expansion and therefore a higher effective pressure drop. Thus, although our one-dimensional model does not take into account the diameter of the test cell, it assumes an experimental apparatus with constant cross-section.

This analysis shows that the velocity U of the flow front is only a function of (1) the pressure ratio (P_1/P_0) and (2) the ratio between the velocities of sound in the mixture and air (C_m/C_0) and does not depend on time. This is the reason why, after an initial acceleration, the flow front maintains an almost constant velocity for a while (Fig. 7). Furthermore, the rarefaction wave that travels through the sample is reflected upward from the bottom of the test cell and reaches the flow front of the expanding bed after a time $t = L(C_m^{-1} + (C_m - U)^{-1})$, which is more than 12 ms in our case, because the wave travels with a velocity of sound C_m approximately equal to 10 m/s in our experimental conditions.

5. Model of the initial velocities of expansion in volcanic conditions

In volcanoes, after the disruption of a rock plug in the conduit or the collapse of a lava dome, a rarefaction wave propagates downward in a bubble-rich magma causing its expansion and fragmentation. In correspondence to this rarefaction wave, the gas–particle dispersion generated by fragmentation expands because the pressure is higher than at the top of the conduit. In this case, Eq. 5b can be used to estimate the initial

velocities of expansion U_v of the generated gas–particle flows. Here P_0 is the volcanic overpressure P_v, that causes the expansion of the fragmented magma. The pressure P can be considered equal to atmospheric (i.e. the pressure at the conduit exit) if we simulate the flow caused by a dome collapse, because the shock wave generated by the removal of the dome at the top of the conduit will be nearly spherical and for this reason its intensity will drop down quickly. Of course, P will be different from atmospheric if we simulate the gas–particle flows caused by a rock plug removal within a volcanic conduit where the shock wave would be flat and so more intense. We have calculated α_0 in Eq. 5b using the following relationships:

$$\alpha_0 = \frac{\rho_p(w_0 - w)}{\rho_p(w_0 - w) + \rho_g(1 - w_0)};$$

$$w = k\sqrt{P_v};\ \rho_g = \frac{P_v}{RT} \qquad (6)$$

that have been obtained from mass balance between melt and bubbles and assuming an equilibrium mass transfer. In these relationships, w_0 and w are respectively the initial magma water content and the magma water content when the pressure is P_v, k is the solubility coefficient, R is the gas constant and T is the temperature.

The initial velocities of expansion U_v are plotted as a function of volcanic overpressure P_v (between 0.1 and 20 MPa) and initial magma water content w_0 (between 0.5 and 5 wt%) for a flow in the atmosphere caused by the collapse of a dome resting at the top of the conduit (Fig. 10A) and for the flow within a volcanic conduit caused by the removal of a rock plug (Fig. 10B). In this second case, the pressure P is the pressure after the shock wave in air calculated by standard equations [11]. The calculations in Fig. 10A can be applied only to the very first moments of expansion because gas–particle flows in the atmosphere are not one-dimensional. Fig. 10 shows that the velocities of the flows in the atmosphere caused by a dome collapse are higher (between approximately 25 and more than 500 m/s) than

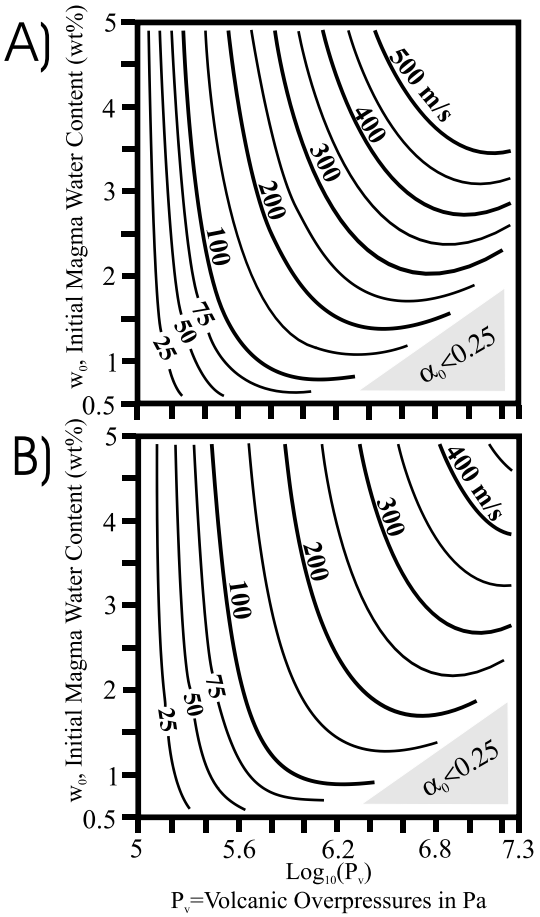

Fig. 10. Initial velocities of expansion U_v of volcanic gas–particle flows calculated using Eq. 5b for (A) the collapse of a dome resting at the top of a conduit (spherical shock wave in the atmosphere) and (B) the removal of a plug in a volcanic conduit (plane shock wave within the conduit). No calculations were performed where $\alpha_0 < 0.25$.

those of the flows in conduits (approximately 25–400 m/s). In any case, these velocity values overestimate the initial velocities of volcanic flow fronts for various reasons. First, the pressure at the top of the body of magma does not drop down immediately because the disruption of the volcanic diaphragm (rock plug or lava dome) requires time. Second, the pressure in the magma also decreases before and during the beginning of fragmentation. Third, the irregular shape and interlocking of the pyroclasts cause friction that reduces the velocities of expansions.

6. Discussion

6.1. Comparison with volcanic explosions

The short-lived decompressions in the shock tube are due to a sudden release of pressure and for this reason are useful to study discrete, cannon-like vulcanian explosions, where vulcanian is a generic term for discrete explosions whose actual causes and characters can vary greatly [6]. Here, we are not simulating magma fragmentation because the material we are using is already fragmented, but the experiments and model investigate the expansion of gas–particle mixtures created immediately after magma fragmentation that follows the disruption of a rock plug in a volcanic conduit or the collapse of a lava dome. Thus, to illustrate the applicability of the study, we review velocities of decompressing volcanic systems in comparable volcanic explosions.

During vulcanian activity, exit velocities from 40 to 170 m/s were observed at the Soufriere Hills volcano, Montserrat [12] and velocities up to 300 m/s were measured in Ngauruhoe volcano suggesting even higher initial values [13,14]. Similar velocities have also been obtained by theoretical models, for example, between 60 and 170 m/s for the explosive decompression of lava domes [15] but also in excess of 300 m/s in a mathematical model of the propagation of an expansion wave within an idealized shock tube that simulates vulcanian activity [16]. Also, Alidibirov [17] obtained velocities in the range 100–250 m/s in his model of the explosive fragmentation of a cryptodome where he assumes an initial gas pore pressure equal to 20 MPa. Woods and co-authors [18] used overpressures of 5–10 MPa in their theoretical work, but in a mathematical model of the Mount St. Helens blast of May 18, 1980 (where observed ejecta velocities reached 250 m/s) overpressures up to 20 MPa were considered [19]. As in our experiments, also during vulcanian explosions the initial motion of the high-velocity conduit flows may be dominated by momentum [6].

Eq. 5b gives predictions that are in good agreement with our experimental data (Fig. 8A), and for volcanic overpressures (Fig. 10) suggests a range of initial velocities of volcanic flows caused by the removal of a rock plug within volcanic conduits between 25 and 400 m/s within which, as shown above, the values obtained with observations and modeling studies are included. In any case, the purpose of our mathematical model is only to estimate the initial velocities of expansion and it does not explain the complex structures that are observable in the expanding beds.

6.2. Features of the expanding beds

The decompressions of these beds display features such as expansions, bubbles and turbulence that are reminiscent of fluidization. For example, in classic fluidization experiments [10], when the velocity of the gases increases, the sample passes through different regimes from particulate fluidization (i.e. expansion with no bubbles), to bubbling fluidization (i.e. expansion with bubbles), to turbulent fluidization and then fast fluidization and dilute transport. Early expansions without bubbles are visible in our experiments as well (Fig. 2), but small voids may not be discernible in the initial stages of the flows simply because they are not resolvable or are in the interior of the flow. In any case, in our experiments the expansion is achieved by the propagation of a rarefaction wave that moves downward from the top to the bottom of the sample (as in volcanic conduits), whereas in traditional fluidization experiments the expansion is generated by gases moving upward from a gas distributor located at the base of the bed. Furthermore, the fluidization characteristics depend on the environmental conditions such as temperature and pressure [10] and our experiments have not been carried out at atmospheric pressure. We also observed sub-horizontal concentrations of gas-rich regions (Figs. 2 and 6), which look like horizontal fractures that partition a portion of the beds into horizontal slabs. This feature, which was also described by Anilkumar [1], is more prominent during the decompressions of the coarser grain size particles.

6.3. Implications for volcanic eruptions

Our experiments generate high-speed, dusty gases, which are the result of rapid depressuriza-

tion of the interstitial bed fluid and the consequent expansion of the bed of particles (Fig. 2). Also the fragmentation of magma may produce expanding gas–particle mixtures with some of the general characteristics observed in our experiments, although some features are probably affected by inter-particle forces such as the electrostatic forces induced by the charges carried by the particles. For example, the two-phase flows are highly inhomogeneous in density (Fig. 3) because of the presence of bubble-like heterogeneities and this is possible in real volcanic flows [1,2,6]. In this case, the bubble-like heterogeneities are probably not significantly affected by the electrostatic forces because bubbles are also present during classical fluidization experiments [10] of coarser grain size particles where the electrostatic forces are clearly not dominant. The complexity of these flows is also demonstrated by their highly irregular flow fronts (Fig. 3), whose finger-like protrusions remind the contemporary, numerous dark-gray finger jets of ash and debris spreading from the vent at the beginning of vulcanian explosions [12].

We advance the hypothesis that large inhomogeneities in density due to the presence of bubble-like heterogeneities are also possible in volcanic conduit flows. In our experiments, the largest bubbles can reach a size that is an important fraction of the diameter of the narrow test cell (Fig. 6). This is a critical issue to understand the dynamics of explosive flows as they emerge from vents, which has been considered in controversial discussions of how pyroclastic flows can form during explosive eruptions. For example, a low particle concentration mixture produces a low density, turbulent gravity current, which either deposits in a dilute state or develops dense underflows. However, if highly inhomogeneous flows emerge then much of the erupted particles will already be in very dense regions. As such regions fall under gravity they can immediately generate concentrated pyroclastic flows during the collapse processes. There will also be much more efficient separation of gas and pyroclasts.

The jets caused by the oscillations of the samples discretize the flows and generate different pulses (Figs. 5 and 6). A question arises then, if a similar mechanism in real volcanoes can produce different, separate flows within the conduits and discrete, pulse-like ejections of gas–particle mixtures out of the vent to generate pyroclastic flows. A difference between real volcanoes and our experimental apparatus is that our shock tube is closed at the top and at the bottom and this causes multiple reflections of rarefaction and compression waves and allows the air still inside the tube at small Δp to oscillate. For this reason, we have focused our velocity measurements and quantitative model to the early stages of the expansion. Furthermore, the jets caused by the oscillations of the coarser grain size particles are smaller in size than those generated by the finer particles. However, rarefaction resonance occurs in shock-tube flows and this has been suggested to generate pulsed propagation of erupted ash also in volcanic conduits [20]. In magma chambers and volcanic conduits, multiple reflections may be due to density interfaces or variations of the conduit diameter. We can also suggest that oscillations and jets may be caused by gas overpressures generated when the volcanic gas–particle mixture flows back into a conduit that has not been completely emptied. Erupted material that falls back into the conduit may also play a role in eruption pulsations by creating momentary plugs or restrictions with re-circulation of the previously expelled tephra.

Acknowledgements

The first author was supported by a Fellowship provided by the European Community (EU Volcano Research Network). A.B. and O.M. are supported by a grant of the Russian Foundation for Basic Research (02-01-00067). R.S.J.S. is supported by a NERC Professorship. We are grateful to Prof. D. Dingwell, Dr. S. Lane and an anonymous reviewer, who provided useful and constructive comments.***[BOYLE]***

References

[1] A.V. Anilkumar, Experimental studies of high-speed

dense dusty gases, PhD Thesis, California Institute of Technology, Pasadena, CA, 1989, 119 pp.
[2] A.V. Anilkumar, R.S.J. Sparks, B. Sturtevant, Geological implications and applications of high-velocity two-phase flow experiments, J. Volcanol. Geotherm. Res. 56 (1993) 145–160.
[3] I. Sugioka, M. Bursik, Explosive fragmentation of erupting magma, Nature 373 (1995) 689–692.
[4] H.M. Mader, J.C. Phillips, R.S.J. Sparks, B. Sturtevant, Dynamics of explosive degassing of magma: observations of fragmenting two-phase flows, J. Geophys. Res. 101 (1996) 5547–5560.
[5] H.M. Mader, E.E. Brodsky, D. Howard, B. Sturtevant, Laboratory simulations of sustained volcanic eruptions, Nature 388 (1997) 462–464.
[6] R.S.J. Sparks, M.I. Bursik, S.N. Carey, J.S. Gilbert, L.S. Glaze, H. Sigurdsson, A.W. Woods, Volcanic Plumes, John Wiley and Sons, Chichester, 1997, 574 pp.
[7] S.W. Kieffer, B. Sturtevant, Laboratory studies of volcanic jets, J. Geophys. Res. 89 (1984) 8253–8268.
[8] C. Jaupart, S. Vergniolle, Laboratory models of Hawaiian and Strombolian eruptions, Nature 331 (1988) 58–60.
[9] S.J. Lane, B.A. Chouet, J.C. Phillips, P. Dawson, G.A. Ryan, E. Hurst, Experimental observations of pressure oscillations and flow regimes in an analogue volcanic system, J. Geophys. Res. 106 (2001) 6461–6476.
[10] L.S. Fan, C. Zhu, Principles of Gas-solid Flows, Cambridge University Press, Cambridge, 1998, 557 pp.
[11] L.D. Landau, E.M. Lifshitz, Fluid Mechanics, Butterworth-Heinemann, London, 1995, 552 pp.
[12] T.H. Druitt, S.R. Young, B. Baptie, E.S. Calder, A.B. Clarke, P.D. Cole, C.L. Harford, R.A. Herd, R. Luckett, G. Ryan, B. Voight, Episodes of repetitive vulcanian explosions and fountain collapse at Soufriere Hills Volcano, Montserrat, in: T.H. Druitt, B.P. Kokelaar (Eds.), The Eruption of Soufriere Hills Volcano, Montserrat, from 1995 to 1999, Geological Society Memoir No. 21, London, 2002.
[13] S. Self, L. Wilson, I.A. Nairn, Vulcanian eruption mechanisms, Nature 277 (1979) 440–443.
[14] I.A. Nairn, S. Self, Explosive eruptions and pyroclastic avalanches from Ngauruhoe in February 1975, J. Volcanol. Geotherm. Res. 3 (1978) 39–60.
[15] J.H. Fink, S.W. Kieffer, Estimate of pyroclastic flow velocities resulting from explosive decompression of lava domes, Nature 363 (1993) 612–615.
[16] D.L. Turcotte, H. Ockendon, J.R. Ockendon, S.J. Cowley, A mathematical model of vulcanian eruptions, Geophys. J. Int. 103 (1990) 211–217.
[17] M.A. Alidibirov, A model for the mechanism of the May 18, 1980 Mount St. Helens blast, J. Volcanol. Geotherm. Res. 66 (1995) 217–225.
[18] A.W. Woods, R.S.J. Sparks, J. Batey, C. Gladstone, L.J. Ritchie, M. Bursik, The generation of vertically stratified pyroclastic density currents by rapid decompression of a pressurized lava dome on 26 December (Boxing Day) 1997 at Soufriere Hills Volcano, Montserrat, in: T.H. Druitt, B.P. Kokelaar (Eds.), The Eruption of Soufriere Hills Volcano, Montserrat, from 1995 to 1999, Geological Society Memoir No. 21, London, 2002.
[19] J.C. Eichelberger, D.B. Hayes, Magmatic model for the Mount St. Helens blast of May 18, 1980, J. Geophys. Res. 87 (1982) 7727–7738.
[20] K.H. Wohletz, T.R. McGetchin, M.T. Sandford, E.M. Jones, Hydrodynamic aspects of caldera-forming eruptions: numerical models, J. Geophys. Res. 89 (1984) 8269–8285.